EARTHQUAKE ENGINEERING AND STRUCTURAL DYNAMICS
Earthquake Engng Struct. Dyn. 2006; **35**:1403–1424
Published online 19 June 2006 in Wiley InterScience (www.interscience.wiley.com). DOI: 10.1002/eqe.589

Behaviour of the double concave Friction Pendulum bearing

Daniel M. Fenz[‡,¶] and Michael C. Constantinou[*,†,§]

Department of Civil, Structural and Environmental Engineering, 212 Ketter Hall, State University of New York at Buffalo, Buffalo, NY 14260, U.S.A.

SUMMARY

The double concave Friction Pendulum (DCFP) bearing is an adaptation of the well-known single concave Friction Pendulum bearing. The principal benefit of the DCFP bearing is its capacity to accommodate substantially larger displacements compared to a traditional FP bearing of identical plan dimensions. Moreover, there is the capability to use sliding surfaces with varying radii of curvature and coefficients of friction, offering the designer greater flexibility to optimize performance. This paper describes the principles of operation of the bearing and presents the development of the force–displacement relationship based on considerations of equilibrium. The theoretical force–displacement relationship is then verified through characterization testing of bearings with sliding surfaces having the same and then different radii of curvature and coefficients of friction. Lastly, some practical considerations for analysis and design of DCFP bearings are presented. Copyright © 2006 John Wiley & Sons, Ltd.

Received 10 October 2005; Revised 19 February 2006; Accepted 11 April 2006

KEY WORDS: double concave Friction Pendulum bearing; seismic isolation

1. INTRODUCTION

The double concave Friction Pendulum (DCFP) bearing consists of two facing concave stainless-steel surfaces. The upper and lower concave surfaces have radii of curvature R_1 and R_2, respectively, which may be unequal. The coefficients of friction of the concave surfaces are μ_1 and μ_2, respectively, which are also not necessarily equal. An articulated slider faced with a non-metallic sliding material separates the two surfaces. The articulation is necessary for proper

*Correspondence to: Michael C. Constantinou, Department of Civil, Structural and Environmental Engineering, 212 Ketter Hall, State University of New York at Buffalo, Buffalo, NY 14260, U.S.A.
†E-mail: constan1@eng.buffalo.edu
‡E-mail: dmfenz@buffalo.edu
§Professor.
¶Ph.D. Student.

Contract/grant sponsor: Multidisciplinary Center for Earthquake Engineering Research; contract/grant number: 8.2.1

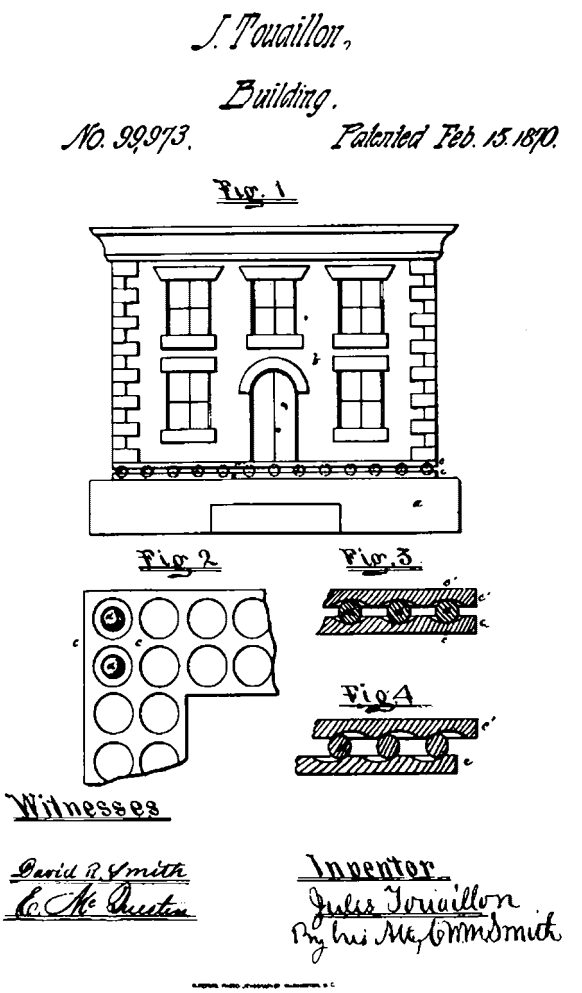

Figure 1. Jules Touaillon's original patent for a double concave rolling ball bearing.

distribution of pressure on the sliding interface and to accommodate differential movements along the top and bottom sliding surfaces.

The concept of a double concave bearing represents the first documented proposal for a seismic isolation system. Figure 1 shows the 1870 U.S. patent of Jules Touaillon that describes a double concave rolling ball bearing [1]. Hyakuda *et al.* [2] presented the description and observed response of a seismically isolated building in Japan which utilized DCFP bearings. The bearing used in Japan is what is shown in Figure 2(a) with equal radii concave surfaces, but with a slider that lacks articulation. Articulation is needed to (a) accommodate differential rotations of the slider top and bottom parts when friction is unequal on the two sliding interfaces and to (b) evenly distribute load on the contact surface and avoid excessive wear. Tsai *et al.* [3–6] described a similar spherical double concave sliding isolation system with articulated slider called the multiple

DOI: 10.1002/eqe

Friction Pendulum system. Experimental and analytical results on the behaviour of a system having concave surfaces of equal radii and equal coefficients of friction at the top and bottom sliding surfaces were presented.

This paper describes the behaviour of the DCFP bearing in a way that is distinct from previous studies. The presentation is largely based on the report of Constantinou [7] available through the Network for Earthquake Engineering Simulation (NEES). The previous studies of Hyakuda *et al.* [2] and Tsai *et al.* [3–6] described the lateral force–displacement relationship of the bearing under conditions restricted to simultaneous sliding on both concave surfaces. This paper provides a more general description of the behaviour of the DCFP bearing that accounts for (a) unequal radii of curvature of the two concave surfaces, (b) unequal coefficients of friction of the two sliding interfaces, (c) effect of the height of the articulated slider on the lateral force–displacement relation and (d) effect of friction in the rotational part of the articulated slider on the lateral force–displacement relation. Previous studies have not addressed these issues.

In addition, experimental results on the behaviour of model DCFP bearings are presented and compared to theoretical predictions. The experiments include four cases of bearing configuration, (a) equal radii and equal coefficients of friction, (b) equal radii and unequal coefficients of friction, (c) unequal radii and equal coefficients of friction and (d) unequal radii and unequal coefficients of friction. The presented results demonstrate a more complex behaviour of DCFP bearing than previously thought. The lateral force–displacement relation of the bearing is shown to have a behaviour ranging from rigid-linear hysteretic to rigid-bilinear hysteretic depending on the selection of the radii of curvature and the friction coefficients.

2. FORCE–DISPLACEMENT RELATIONSHIP FOR THE DCFP BEARING

Figure 2 presents cross sections through a DCFP bearing at various stages of displacement. Figure 2(a) shows a bearing at zero displacement and establishes the nomenclature used. Figure 2(b) shows the bearing undergoing sliding on the lower concave surface only, a behaviour that is possible when the coefficient of friction on the lower sliding interface is less than the coefficient of friction on the upper sliding interface. Movement such as shown in Figure 2(b) requires rotation of the articulated slider. Given that friction cannot exactly be the same at the two sliding interfaces, there is always some rotation of the slider. This demonstrates the significance of articulation, without which, the slider would be subject to uneven wear. The maximum displacement capacity of the bearing is $2d$, where d is the maximum displacement capacity of a single concave surface. This is shown in Figure 2(c). Note that due to rigid body and relative rotation of the slider, the displacement capacity is actually slightly different than $2d$.

To derive the force–displacement relationship for the DCFP bearing, the motions of the top and bottom surfaces are considered separately and then combined based on equilibrium and compatibility to yield the relationship for the complete bearing. It is assumed in the formulation of the governing equations that the concave plates have sufficient displacement capacity so that the slider does not impact the retainer ring. Examining the free body diagram of the slider on the top concave surface in the deformed configuration shown in Figure 3, the forces acting on the slider are:

1. The vertical load, W, acting at the pivot point.
2. The lateral force, F_1, transferred through the bottom part of the bearing and acting on the top part of the slider.

DOI: 10.1002/eqe

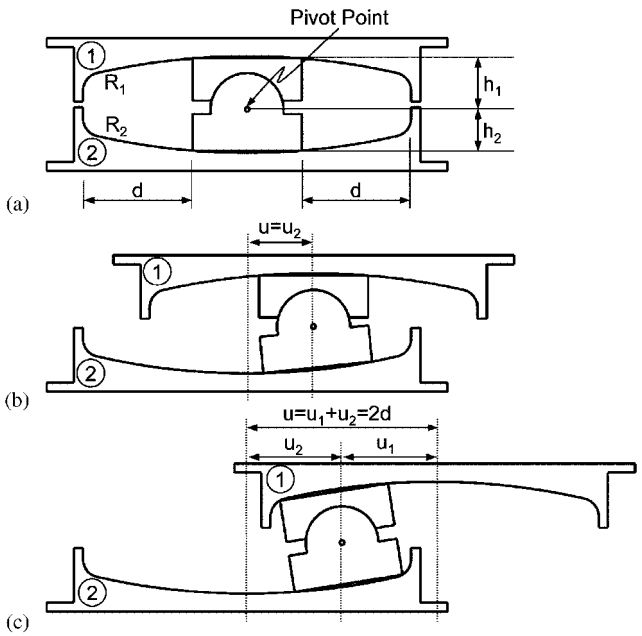

Figure 2. Section through centre of DCFP bearing at various stages of motion.

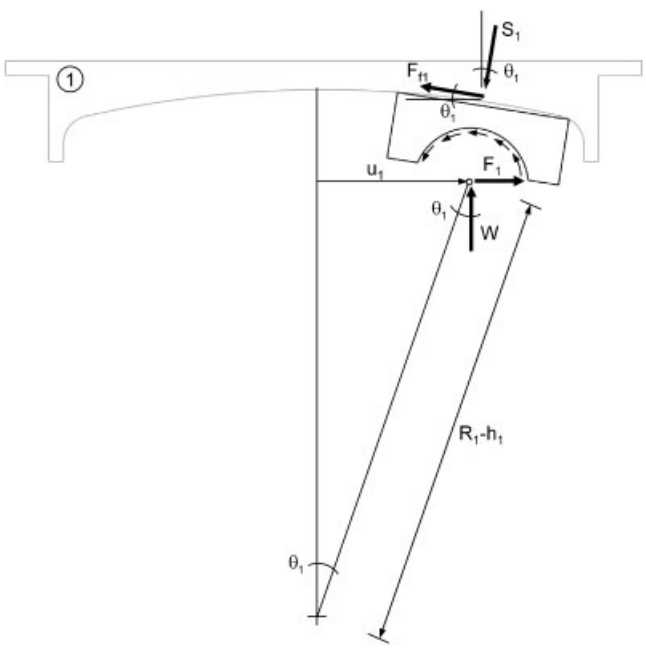

Figure 3. Free body diagram of slider on upper concave surface in the deformed configuration.

DOI: 10.1002/eqe

3. The friction force, F_{f1}, acting along the sliding interface.
4. The resultant force of normal pressure acting on the sliding interface, S_1. This must be off centre to satisfy moment equilibrium. Accordingly, the pressure distribution on the sliding interface is not uniform.
5. Friction tractions along the spherical surface of the articulated slider. These tractions appear only when there is rotation of the articulated slider. This situation occurs only when friction is unequal at the two sliding interfaces, regardless of whether the two concave surfaces have equal or unequal radii of curvature.

Considering equilibrium in the horizontal and vertical directions, the following relationships are obtained:

$$F_1 - S_1 \sin\theta_1 - F_{f1} \cos\theta_1 = 0 \tag{1}$$

$$W - S_1 \cos\theta_1 + F_{f1} \sin\theta_1 = 0 \tag{2}$$

Note that in Equations (1) and (2) the friction tractions do not appear. Their effect is assumed to be part of the friction force F_{f1}.

From geometry, the displacement of the slider on the top concave surface, u_1 is

$$u_1 = (R_1 - h_1) \sin\theta_1 \tag{3}$$

where $R_1 - h_1$ is the distance from the centre of the spherical surface to the pivot point of the articulated slider.

Combining Equations (1), (2) and (3), the force–displacement relationship that governs motion on one concave sliding surface is the force–displacement relationship for the traditional FP bearing

$$F_1 = \frac{W}{(R_1 - h_1)\cos\theta_1} u_1 + \frac{F_{f1}}{\cos\theta_1} \tag{4}$$

Similar analysis of equilibrium for sliding on the bottom concave surface yields

$$F_2 = \frac{W}{(R_2 - h_2)\cos\theta_2} u_2 + \frac{F_{f2}}{\cos\theta_2} \tag{5}$$

where F_2 is the force transferred through the top part of the bearing and acting on the bottom slider, u_2 is the displacement of the slider along the bottom concave surface, F_{f2} is the friction force acting along the bottom sliding surface and θ_2 is the angle of rotation of the bottom part of the articulated slider.

Typically, the radii of curvature are large compared to the displacements u_1 and u_2 such that angles θ_1 and θ_2 are small and the following simplifications can be made with negligible loss of accuracy:

$$F_1 = \frac{W}{R_1 - h_1} u_1 + F_{f1} \tag{6}$$

$$F_2 = \frac{W}{R_2 - h_2} u_2 + F_{f2} \tag{7}$$

Equations (6) and (7) govern the force–displacement relationship for the top and bottom sliding surfaces, respectively. The significance of the height of the articulated slider becomes apparent

DOI: 10.1002/eqe

in Equations (6) and (7). Note that these equations also apply for the single concave FP bearing. FP bearings (whether single or double concave) carrying large loads have substantial size sliders, which influence their behaviour.

For the entire bearing, u, the total displacement (top plate relative to bottom plate) is the sum of the displacements on the top and bottom surfaces:

$$u = u_1 + u_2 \tag{8}$$

Furthermore, considering equilibrium of the slider in the horizontal direction (and excluding the insignificant inertia forces associated with the moving parts of the bearing):

$$F = F_1 = F_2 \tag{9}$$

Using Equations (6)–(9), the force–displacement relationship for the entire bearing is

$$F = \left(\frac{W}{R_1 + R_2 - h_1 - h_2}\right) u + \left(\frac{F_{f1}(R_1 - h_1) + F_{f2}(R_2 - h_2)}{R_1 + R_2 - h_1 - h_2}\right) \tag{10}$$

and the individual displacements on each sliding surface are

$$u_1 = \left(\frac{F - F_{f1}}{W}\right)(R_1 - h_1) \tag{11}$$

$$u_2 = \left(\frac{F - F_{f2}}{W}\right)(R_2 - h_2) \tag{12}$$

Equation (10), which was originally presented by Tsai *et al.* [3–6] except for the effect of the slider's height, is valid only when sliding is simultaneously occurring on both concave surfaces. Consider the case where friction at the sliding interfaces is unequal, say $F_{f1} < F_{f2}$. Upon application of lateral force, F, such that $F_{f1} < F < F_{f2}$, sliding will occur only on the surface of least friction. Motion will continue along only surface 1 ($u_1 = u, u_2 = 0$) until $F = F_{f2}$, when sliding will commence on both surfaces. This occurs at a displacement u^*, given by

$$u^* = (\mu_2 - \mu_1)(R_1 - h_1) \tag{13}$$

where $\mu_1 = F_{f1}/W$ and $\mu_2 = F_{f2}/W$ are the coefficients of friction ($\mu_1 < \mu_2$) at the two sliding interfaces. Therefore, Equation (10) is valid only when $u \geqslant u^*$. When $u < u^*$, the force–displacement relationship is governed by Equation (6) when $\mu_1 < \mu_2$ and Equation (7) when $\mu_2 < \mu_1$. The generalized force–displacement behaviour for the case when $\mu_1 < \mu_2$ is presented in Figure 4.

Upon sliding on both concave surfaces, the strength of the bearing is equal to $\mu_e W$, where μ_e is the effective coefficient of friction. It is derived from the second term of Equation (10) by dividing by the vertical load, W:

$$\mu_e = \frac{\mu_1(R_1 - h_1) + \mu_2(R_2 - h_2)}{R_1 + R_2 - h_1 - h_2} \tag{14}$$

An interesting observation may be made by deriving expressions for the angles of rotation θ_1 and θ_2 (see Figure 3). Angle θ_1 is the angle of rotation of the top part of the articulated slider and θ_2 is the angle of rotation of the bottom part. When $\theta_1 = \theta_2$, the articulated slider moves as

DOI: 10.1002/eqe

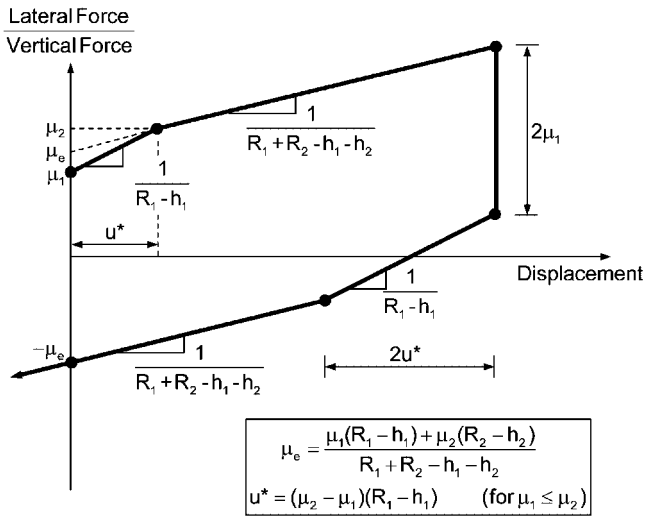

Figure 4. General normalized force–displacement relationship for DCFP bearing with $\mu_1 \leqslant \mu_2$.

a rigid body without relative rotation. Based on the geometry of Figure 3 and use of Equation (11), θ_1 is given by

$$\theta_1 = \sin^{-1}\left(\frac{u_1}{R_1 - h_1}\right) = \sin^{-1}\left(\frac{F - F_{f1}}{W}\right) \tag{15}$$

Similarly, using Equation (12), θ_2 is given by

$$\theta_2 = \sin^{-1}\left(\frac{u_2}{R_2 - h_2}\right) = \sin^{-1}\left(\frac{F - F_{f2}}{W}\right) \tag{16}$$

Therefore, when the friction forces at the two sliding interfaces are equal and irrespective of whether the two surfaces have equal or unequal radii, the angles of rotation are equal and the slider does not experience relative rotation.

As an illustrative example, consider a DCFP bearing with $R_1 - h_1 = 1000$ mm, $R_2 - h_2 = 3000$ mm, $\mu_1 = 0.03$ and $\mu_2 = 0.06$ that is subjected to one full cycle of motion with 150 mm amplitude. This configuration is representative of a bearing having significant restoring force and re-centring capability for weak excitations, yet still with adequate flexibility to achieve desirable performance for strong excitations. The complete force–displacement relationship is presented in Figure 5.

Starting from rest (Point 0 in Figure 5), motion will begin on the surface of least friction when the lateral force exceeds the breakaway force, $\mu_1 W$ (Point 1). At this point, the lateral force is not large enough to initiate motion on surface 2 and sliding occurs only on surface 1 ($u_2 = 0$ and the stiffness is inversely proportional to $R_1 - h_1$). At total displacement $u^* = 30$ mm, there is sufficient force to initiate sliding on surface 2 and motion progresses with sliding on both surfaces to the maximum displacement (Point 2 to Point 3) with stiffness inversely proportional to $R_1 + R_2 - h_1 - h_2$. It should be noted that at maximum total displacement, the peak displacements

DOI: 10.1002/eqe

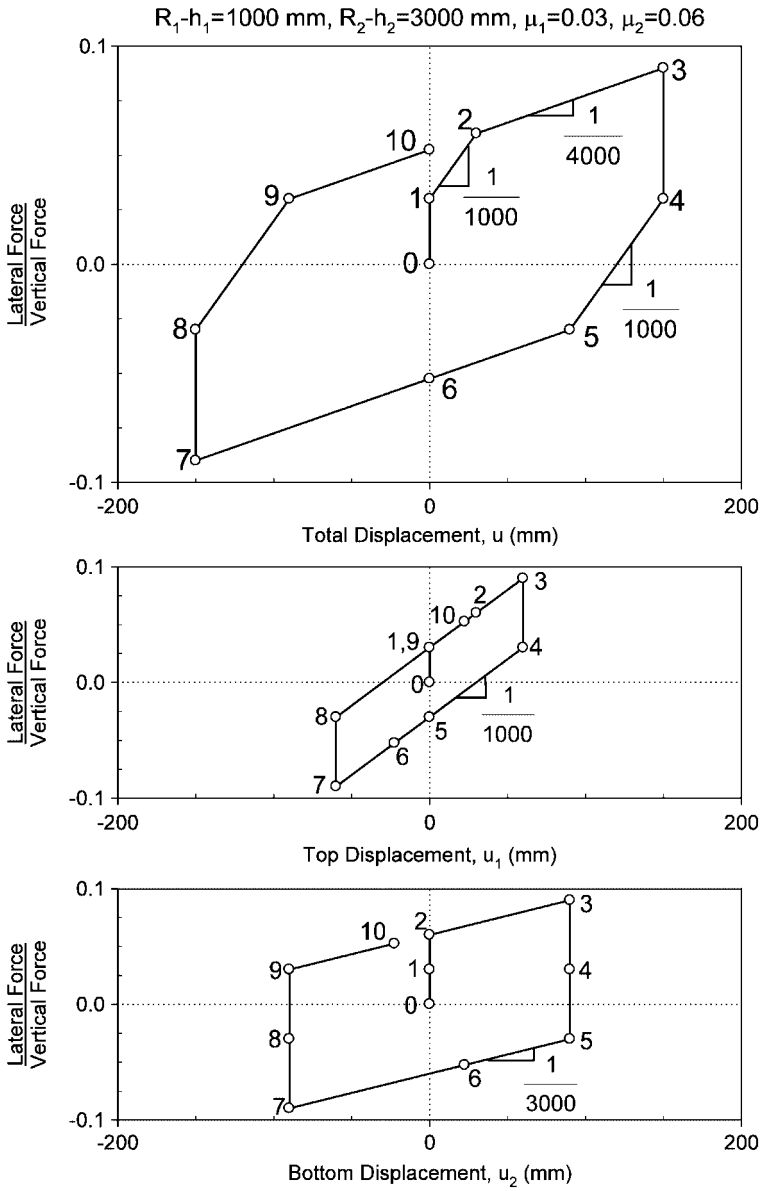

Figure 5. Example hysteresis loops for a configuration of DCFP bearing having unequal radii of curvature and unequal coefficients of friction.

on each sliding surface are unequal ($u_{1\,\max} = 60\,\text{mm}$ and $u_{2\,\max} = 90\,\text{mm}$) due to the different radii and values of friction.

Upon reversal of motion, the lateral force drops by $2\mu_1 W$ when motion begins in the opposite direction on surface 1. However, the lateral force must drop by $2\mu_2 W$ for sliding to initiate on

DOI: 10.1002/eqe

surface 2. Therefore, upon reversal of motion, the bearing will slide only on surface 1 and the stiffness will be inversely proportional to $R_1 - h_1$ (Point 4 to Point 5). After a distance $2u^*$, sliding initiates on surface 2 and the stiffness becomes inversely proportional to $R_1 + R_2 - h_1 - h_2$ (Point 5 to Point 7). Due to the different radii and coefficients of friction at each sliding surface, the displacements on each surface are both non-zero when the total displacement is zero (Point 6 and Point 10). This will be discussed in more detail later.

When the normalized lateral force is plotted against the component of sliding displacement on a single surface, the resulting hysteresis loop is that of a single concave FP bearing having the same radius of curvature and coefficient of friction as that surface. Therefore, the overall force–displacement relationship for the DCFP bearing can be obtained by considering two single concave FP bearings acting in series. From equilibrium of the articulated slider, the horizontal forces F_1 and F_2 must be equal (except for the insignificant effect of the inertia force of the slider), though the displacements on each surface are not.

The behaviour depicted in Figures 4 and 5 assumes that the friction coefficient at each sliding interface is constant. In reality, the coefficient of friction exhibits velocity dependence [8]. Moreover, the friction force may be affected by contributions from friction tractions in the articulated slider. These effects will become apparent in test results to be presented next.

3. EXPERIMENTAL TESTING AND RESULTS

With the theoretical force–displacement relationship for the DCFP bearings established, characterization testing was performed to confirm the theoretical predictions. Testing of the two DCFP bearings shown in Figure 6 was performed using the bearing testing machine in the Structural Engineering and Earthquake Simulation Laboratory at the University at Buffalo [9].

3.1. Testing of DCFP bearing with concave surfaces of equal radii

The first test specimen had two 229 mm diameter concave surfaces each with a 474 mm radius of curvature. However, due to small differences in the height of the two parts of the slider (refer to Figure 6), the effective radii $R_1 - h_1$ and $R_2 - h_2$, were 438 and 442 mm, respectively. The diameter of the articulated slider used was 75 mm, yielding an overall displacement capacity of 154 mm. The articulated slider is faced with a woven material similar to the one identified as PTFE Composite 1 by Constantinou *et al.* [8]. To instrument the articulated slider and allow for visual observation during testing, the retainer ring was machined down.

Tests were conducted under a constant vertical load with three fully reversed cycles of sinusoidal motion at 100 mm amplitude and 0.10 Hz frequency, resulting in a peak velocity of 63 mm/s. This is the velocity of the top bearing part with respect to the bottom part; it is not the peak sliding velocity. The peak sliding velocities were about or larger than 25 mm/s (the friction material used typically exhibits peak friction at sliding velocities exceeding about 25 mm/s). Accordingly, during testing the effects of the velocity dependence of friction were apparent.

The frictional conditions were varied during the various tests. In one configuration, the bearing was tested with the two sliding interfaces having nearly identical frictional properties. In another configuration, the bottom surface of the articulated slider was coated with a silicone lubricant so that the two sliding surfaces had substantially different coefficients of friction. To achieve effective lubrication, the radius of curvature of the slider at its upper and lower surfaces was manufactured

DOI: 10.1002/eqe

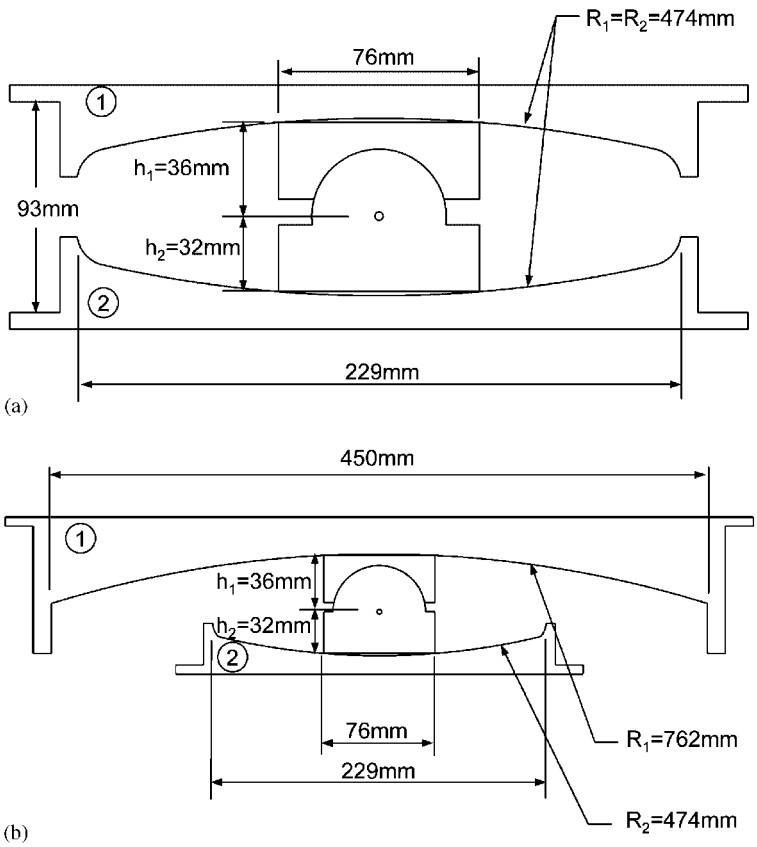

Figure 6. Specimens with concave surfaces: (a) having equal radii of curvature; and (b) unequal radii of curvature used in characterization testing.

larger than the radius of the mating concave surface. This resulted in bearing only over an annular area on the perimeter of the slider as approximately shown in Figure 6. Thus, the sliding interfaces contained a pocket that effectively contained the lubricant.

Figures 7 and 9 present the recorded hysteresis loops and histories of displacement and velocity for the case of the two surfaces having nearly identical friction. In Figure 7, both the overall and decomposed hysteresis loops are presented. The values of friction coefficient shown are those identified in the experiments. The velocity histories presented were obtained through numerical differentiation of the displacement data. Since any noise in the data tends to be amplified by numerical differentiation, the velocity was obtained by differentiating a second-order polynomial that was fit through successive five point windows of displacement data. The resulting velocity data were then smoothed using Gaussian weighting to obtain the plots presented.

The analytical loops presented were constructed based on Equations (6)–(14) using the actual values of $R_1 - h_1$ and $R_2 - h_2$ and the measured values of the friction coefficients μ_1 and μ_2. The analytical and experimental results are in good agreement except that (a) the velocity dependence evidenced in the experimental loops at maximum displacement are not incorporated in

DOI: 10.1002/eqe

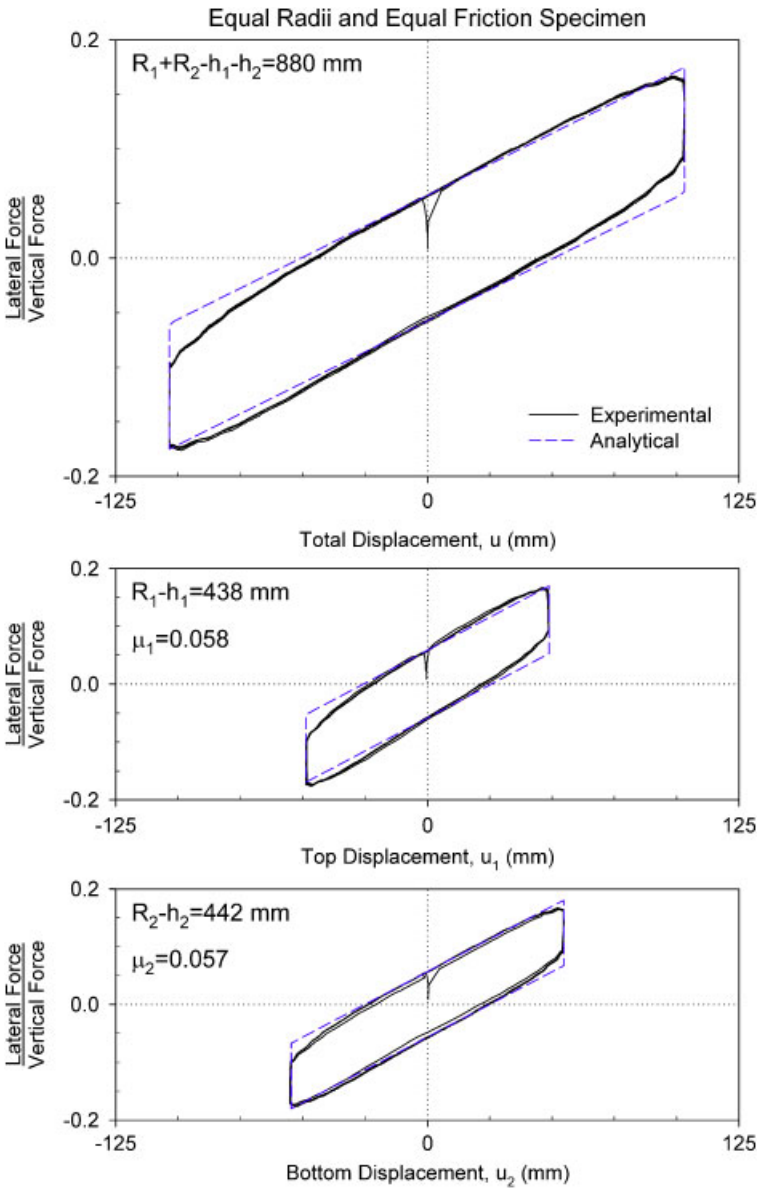

Figure 7. Comparison of experimental and analytical hysteresis loops for specimen with equal radii and equal friction.

the analytical model and (b) the displacements and velocities at the two sliding interfaces are slightly different than what the theory predicts. The primary contribution to this difference is the effect of the articulated slider rotation on the measurement of displacement. The displacement of the slider should have been measured at the pivot point, however this was not possible and the

DOI: 10.1002/eqe

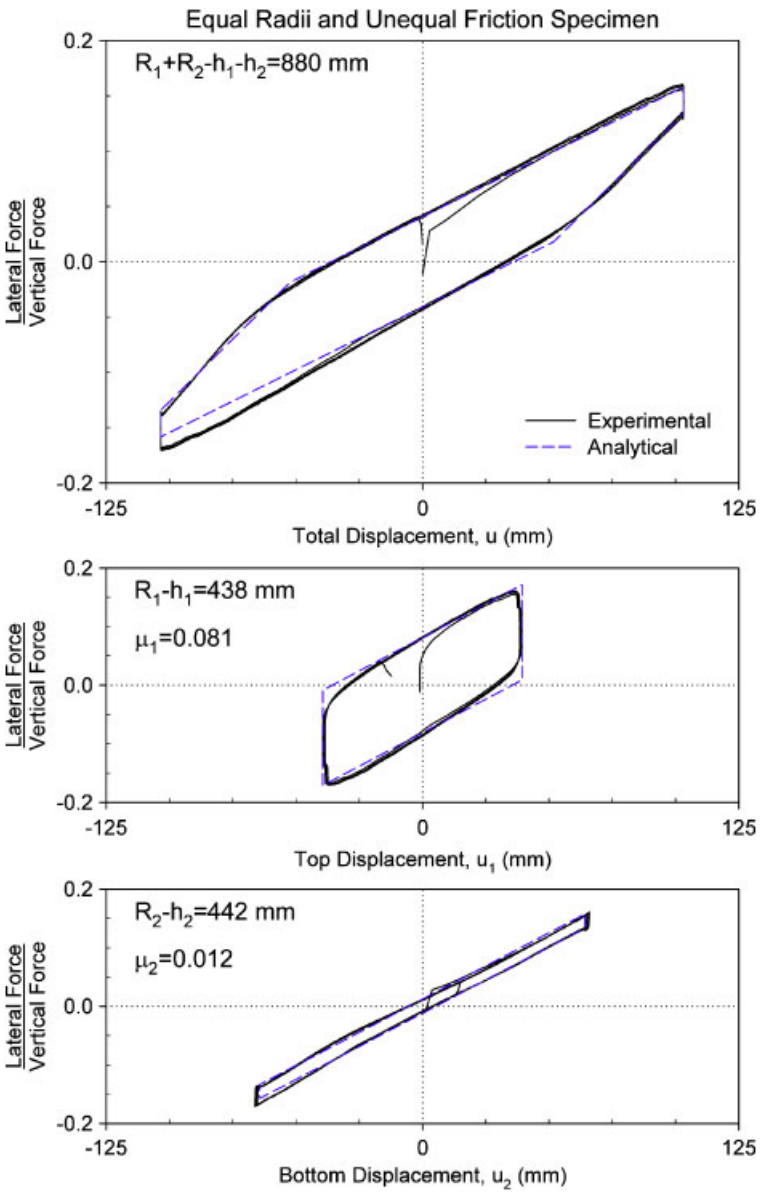

Figure 8. Comparison of experimental and analytical hysteresis loops for specimen with equal radii and unequal friction.

string pot displacement transducer was placed slightly higher than the pivot point. This results in slight under-measurement of displacement u_1 and slight over-measurement of displacement u_2, as evidenced in Figure 9.

The behaviour of the bearing is altered significantly when the coefficients of friction on each surface are different. In Figures 8 and 9, data are presented for a test performed with

DOI: 10.1002/eqe

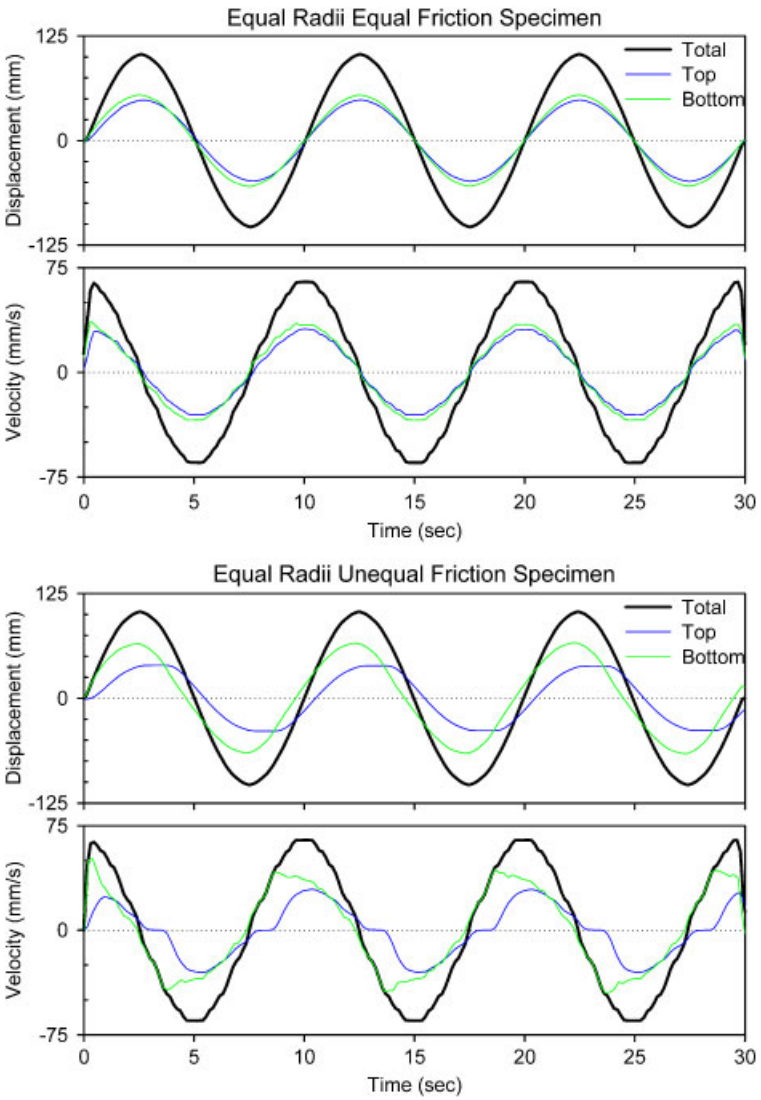

Figure 9. Recorded histories of displacement and velocity for specimen with equal radii.

the bottom part of the slider lubricated as previously described. Also shown in Figure 8 are the analytical loops constructed on the basis of Equations (6)–(14) using the experimentally measured values of friction $\mu_1 = 0.081$ and $\mu_2 = 0.012$. The analytical loops are in good agreement with those measured experimentally, except that the experimental force–displacement loops show asymmetry with more friction force when displacement is negative. This may also be detected in the experimental force–displacement loops for the lower interface, so that a contributor to this behaviour may have been actual asymmetry in the friction of the lower

DOI: 10.1002/eqe

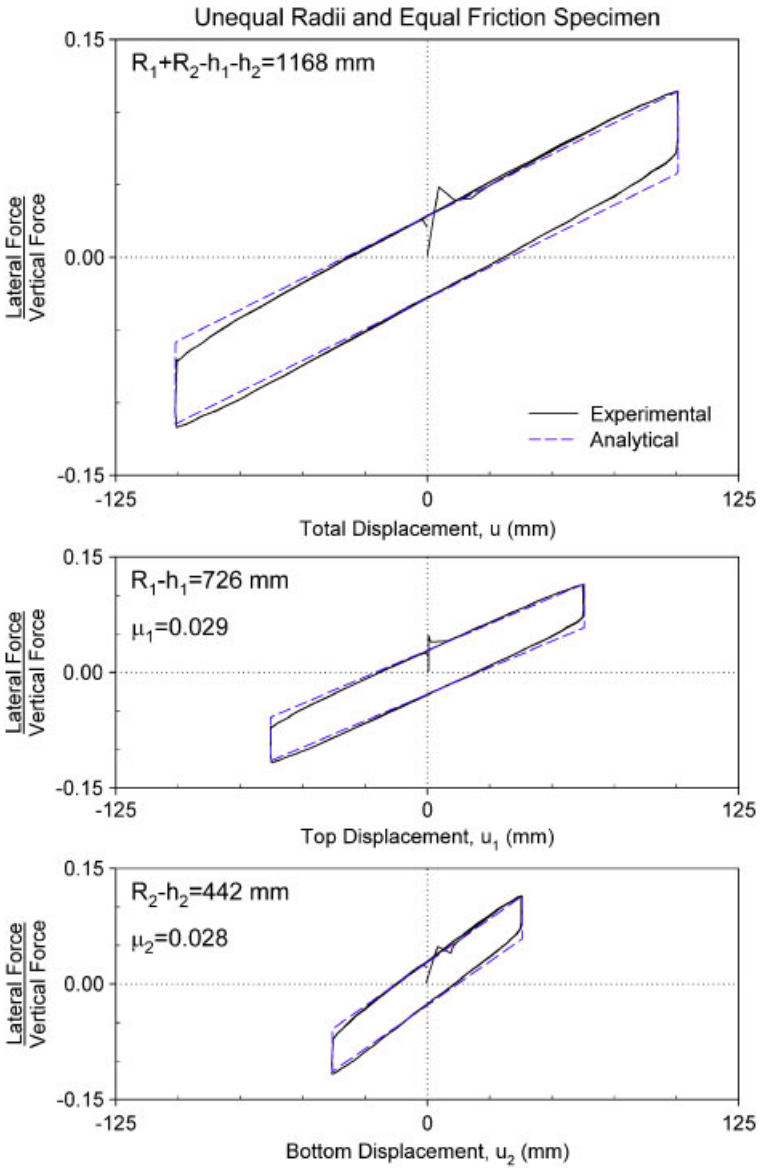

Figure 10. Comparison of experimental and analytical hysteresis loops for specimen with unequal radii and equal friction.

interface. Moreover, the aforementioned error in displacement measurement may have contributed as well.

The histories of displacement and velocity show that upon reversal of motion, sliding only occurs on the surface of least friction. The velocity on the top surface is temporarily zero when the motion is reversed, as the friction on the bottom surface is less.

DOI: 10.1002/eqe

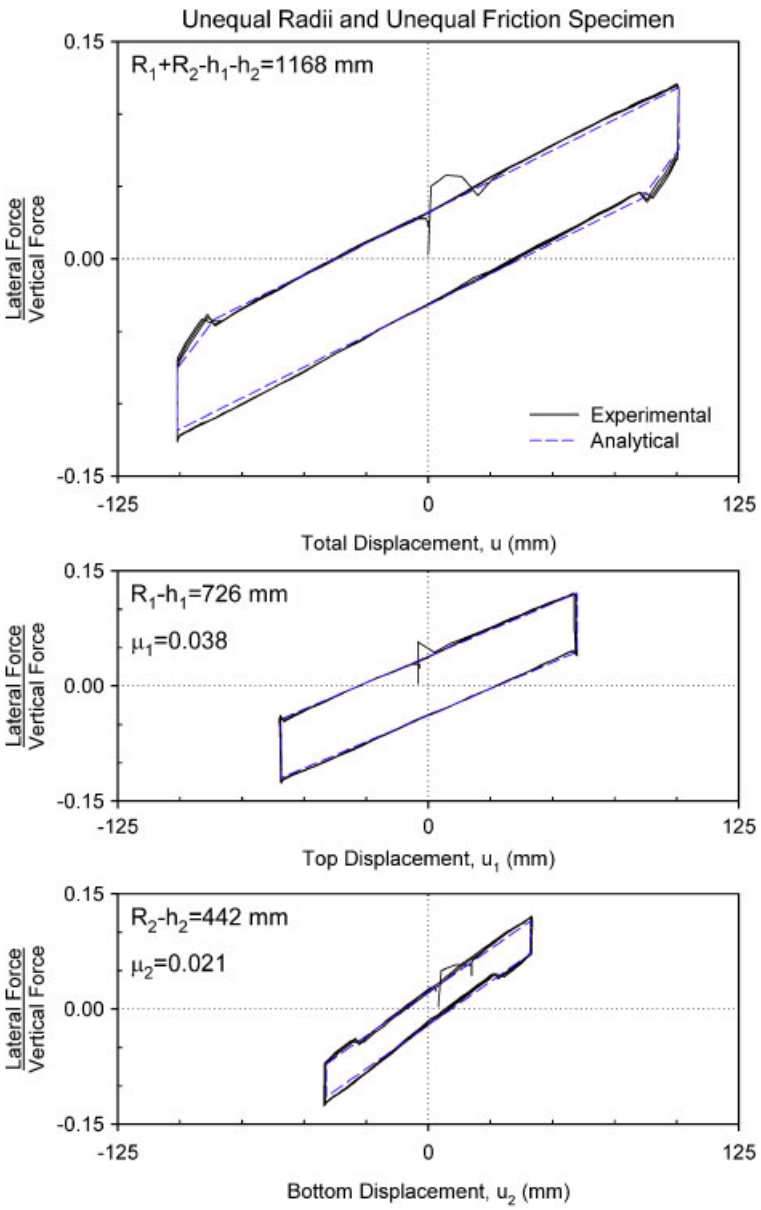

Figure 11. Comparison of experimental and analytical hysteresis loops for specimen with unequal radii and unequal friction.

3.2. Testing of DCFP bearing with concave surfaces of different radii

The second configuration tested had an upper concave surface with $R_1 = 762$ mm and a lower concave surface with $R_2 = 474$ mm. Three fully reversed cycles of sinusoidal motion with 100 mm amplitude and 0.10 Hz frequency were imposed under constant vertical load. When the coefficients

DOI: 10.1002/eqe

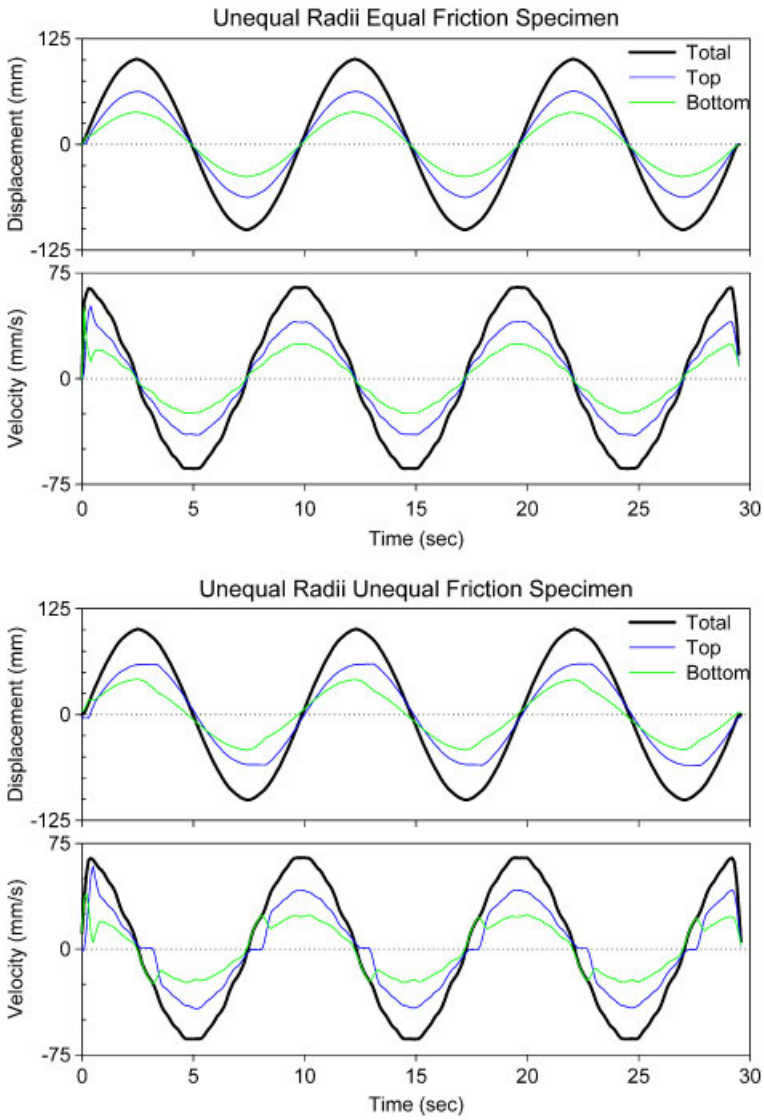

Figure 12. Recorded histories of displacement and velocity for specimen with unequal radii.

of friction on each surface are equal, the behaviour is rigid-linear hysteretic as shown in Figure 10, where again the experimentally obtained values of the coefficients of friction are shown. Though there is simultaneous sliding on each surface over the full course of motion due to equal friction, the displacement amplitudes on each surface differ due to the different radii. The analytical loops, constructed on the basis of Equations (6)–(14) and the experimental values of μ_1 and μ_2 are in good agreement with the experimental loops.

Figure 11 presents force–displacement loops for the case when friction is unequal on each surface. The recorded histories of displacement and velocity are shown in Figure 12. The lower value

DOI: 10.1002/eqe

of friction at the bottom sliding interface was achieved with lubrication as previously described. Analytical construction of the lateral force–displacement loops was based on Equations (6)–(14) and using the experimentally determined friction coefficients $\mu_1 = 0.038$ and $\mu_2 = 0.021$. The analytical loops shown in Figure 11 are in good agreement with the experimental loops except for higher friction force during sliding on one surface, which was not considered in the modelling.

In this test, the interface between the two parts of the articulated slider was cleaned of lubricant, which increased the friction tractions at this interface. The effect of these tractions may be seen in the decomposed loop of the bottom part of the bearing in Figure 11. The friction coefficient is seen to be larger than 0.021 during the intervals of motion for which the sliding on the upper surface ceases (upon unloading over a total displacement interval equal to $2u^*$). During this interval, the articulated slider undergoes large relative rotation. When sliding starts at both surfaces, the relative rotation diminishes, resulting in lesser friction traction contribution to the friction force. This interesting behaviour (although not significant) was observed only when the interior of the slider was free of lubrication.

4. CONSIDERATIONS FOR ANALYSIS AND DESIGN

DCFP bearings having concave surfaces of equal radii and equal friction were first applied in Japan on a small number of buildings [2]. To date, there have been no applications of DCFP bearings with different radii or different coefficients of friction. Some issues related to design and implementation of DCFP bearings are presented below.

4.1. P–Δ moment transfer

In the traditional FP bearing, the P–Δ moment (moment resulting from vertical load P through the total bearing displacement Δ) is transferred to the structure or foundation on the side of the concave plate. In contrast, for the DCFP bearing this moment is divided among the two concave plates. The moments transferred to the top and bottom concave plates are $P \cdot u_1$ and $P \cdot u_2$, respectively, where u_1 and u_2 are the displacements on each surface given by Equations (11) and (12). For bearings with $R_1 - h_1 = R_2 - h_2$ and $\mu_1 \approx \mu_2$, the displacements u_1 and u_2 are each effectively equal to $\frac{1}{2}\Delta$ and the moment transferred through each concave plate is $\frac{1}{2}P\Delta$.

4.2. Modelling for dynamic analysis

Various options exist for modelling of DCFP bearings in programs used for response history analysis of seismically isolated structures. For the simplest case of $R_1 - h_1 = R_2 - h_2$ and $\mu_1 \approx \mu_2$, the behaviour of the bearing can be modelled as that of a traditional FP bearing with radius of curvature $R_1 + R_2 - h_1 - h_2$ and coefficient of friction as determined by experiment. The velocity dependence of the coefficient of friction is described by

$$\mu = f_{\max} - (f_{\max} - f_{\min})\, \mathrm{e}^{-\alpha|v|} \tag{17}$$

where v is the sliding velocity, $f_{\max}$ and $f_{\min}$ are the sliding coefficients of friction at large velocity and nearly zero sliding velocity, respectively, and α is a parameter that controls the transition from $f_{\min}$ to $f_{\max}$. Typically, $f_{\max}$ is determined in the prototype bearing testing program and the parameters $f_{\min}$ and α are selected on the basis of available experimental results (e.g. see Reference [8]).

DOI: 10.1002/eqe

As mentioned earlier, the relevant velocities are the sliding velocities on each concave surface, not the total velocity, v. For DCFP bearings of equal radii and friction, the sliding velocities on each surface are equal and have magnitude $\frac{1}{2}v$. Therefore, Equation (17) still applies provided a value $\alpha/2$ is specified. For example, a value of $\alpha = 100$ s/m is often used for traditional FP bearings. To model a DCFP bearing with the same type of sliding interface, the value $\alpha = 50$ s/m should be specified in the analysis program.

For the general case of a DCFP bearing with unequal radii and unequal friction, the behaviour can be modelled using two traditional FP bearing elements acting in series. It was shown earlier that the overall force–displacement relationship can be decomposed into the components on each sliding surface, yielding a hysteresis loop for each concave surface identical to that which would be obtained for a traditional FP bearing with the same radius of curvature and coefficient of friction. Therefore, by defining two separate single concave FP elements with the radii of curvature and coefficients of friction of each concave surface and connecting them in series with a point mass representing the articulated slider, the overall behaviour of the DCFP bearing is obtained. The velocity dependence of the coefficient of friction is still governed by Equation (17), though the velocities of each isolator element represent the true sliding velocities on each surface. Accordingly, the rate parameter α need not be modified.

4.3. Values of property modification factors

The concept of bounding analysis on the basis of system property modification factors or λ-factors is described in Reference [8] and employed in the 1999 AASHTO Guide Specifications for Seismic Isolation Design [10]. The method is a systematic procedure for calculating upper and lower bound values for the mechanical properties of seismic isolators to account for aging, contamination, history of loading, temperature and other effects.

For FP bearings, only the coefficient of friction is affected by the aforementioned effects. The system property modification factors for DCFP bearings are the same as those for traditional FP bearings except for the contamination factor. Separate factors should be considered for the upper and lower concave surfaces, respectively. Anticipating that DCFP bearings will be sealed (as unsealed bearings with a concave stainless-steel surface facing up are not permitted in the AASHTO Guide Specifications [10]), the contamination factors will be $\lambda_{c1} = 1.0$ for the upper (downward facing) surface and $\lambda_{c2} = 1.1$ for the lower (upward facing) surface. When response history analysis is performed with each bearing explicitly modelled as two spherical sliding surfaces in series, the two different contamination factors can be directly utilized in adjusting the properties of each sliding surface. However, when simplified calculations are performed, a contamination factor for the entire system is needed. This factor may be derived on the basis of Equation (14) that combines the contributions of the frictional forces from the two sliding interfaces:

$$\lambda_c = \frac{\lambda_{c1}\mu_1(R_1 - h_1) + \lambda_{c2}\mu_2(R_2 - h_2)}{\mu_1(R_1 - h_1) + \mu_2(R_2 - h_2)} \tag{18}$$

For the typical case of DCFP bearings with equal radii and friction, $\lambda_c = (\lambda_{c1} + \lambda_{c2})/2 = 1.05$.

4.4. Slider offset and permanent displacements

In displacement-controlled tests where the friction on the top and bottom surfaces is unequal, the articulated slider becomes offset inside the bearing. This is evident in Figures 5, 9 and 12 where

DOI: 10.1002/eqe

it can be seen that there are equal and opposite displacements, denoted $\bar{u}$, on the top and bottom surfaces even though the total bearing displacement is zero. That is, $u = 0$, $u_1 = -u_2 = \pm \bar{u}$.

The magnitude of $\bar{u}$ can readily be calculated and expressed in a number of ways. By setting $u_1 = \bar{u}$ and $u_2 = -\bar{u}$ in Equations (6) and (7), respectively, and invoking Equation (9),

$$|\bar{u}| = \frac{|\mu_1 - \mu_2|}{\dfrac{1}{R_1 - h_1} + \dfrac{1}{R_2 - h_2}} \tag{19}$$

Considering the decomposed force–displacement loops, it is clear that $\bar{u}$ is the distance the slider must move as the normalized lateral force changes from μ_e to μ_1 or μ_2. Since the force–displacement relationship is linear with a known slope, $\bar{u}$ can alternatively be expressed in terms of the effective coefficient of friction as

$$\bar{u} = (\mu_e - \mu_1)(R_1 - h_1) \tag{20}$$

$$\bar{u} = (\mu_e - \mu_2)(R_2 - h_2) \tag{21}$$

Equations (20) and (21) establish the convention of positive $\bar{u}$ on the surface of least friction. The slider advances more on the surface of least friction and lags behind on the surface of higher friction.

The magnitude of slider offset does not accumulate from cycle to cycle with continuous cyclic motion. That is, after n cycles of motion, the slider offset is $\bar{u}$, not $n\bar{u}$. By taking a step-by-step approach as was used to construct Figure 5, it can be shown that the hysteresis loops of subsequent cycles retrace the loop obtained from the first cycle. This is corroborated by the records of displacement presented in Figures 9 and 12. The value of $\bar{u}$ using Equation (19) and the experimentally measured values of friction is 15.2 mm for the case of equal radii and unequal friction and 4.7 mm for the case of unequal radii and unequal friction. The values extracted from the displacement histories of these tests are typically within 1 mm of the theoretical value. Furthermore, the experimental values of $\bar{u}$ are constant from cycle to cycle, indicating that the offset does not grow with repeated cycling.

A second issue related to design of the DCFP bearing is the permanent bearing displacement, u_p, that can result after earthquake excitation. The bearing can exist in an equilibrium position of non-zero displacement in which the static friction force balances the restoring force, $F_f = F_r$. For the DCFP bearing, it is possible to have permanent displacements on both sliding surfaces, given by

$$u_{p1} = \mu_{\min,1}(R_1 - h_1) \tag{22}$$

$$u_{p2} = \mu_{\min,2}(R_2 - h_2) \tag{23}$$

where $\mu_{\min,1}$ and $\mu_{\min,2}$ are the coefficients of friction of each sliding surface at very small velocity. These displacements add to give the total possible permanent displacement of the top plate relative to the bottom plate:

$$u_p = \mu_{\min,1}(R_1 - h_1) + \mu_{\min,2}(R_2 - h_2) \tag{24}$$

Comparing Equations (20) and (21) with (22) and (23) it is evident that in all cases, the permanent displacement possible on an individual sliding surface is larger than the offset displacement. Furthermore, the issue of permanent displacements is more critical for DCFP bearings than for traditional FP bearings since there are two sliding surfaces on which the permanent displacements occur.

DOI: 10.1002/eqe

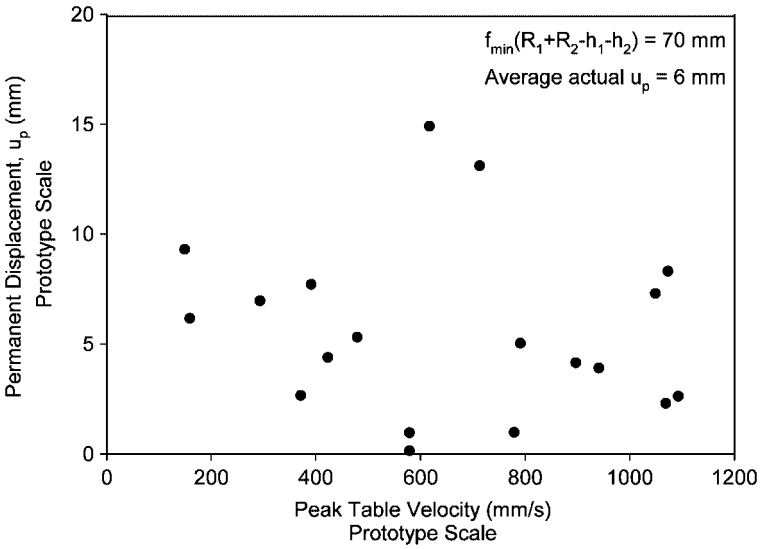

Figure 13. Actual permanent displacements (in prototype scale) measured after 19 unidirectional shaking table tests.

It is important to realize that the value of u_p given by (24) represents the maximum possible permanent displacement. Typically, earthquakes end with a period of very low level excitation which tends to re-centre structures isolated with FP bearings. Past shaking table tests of structures isolated with traditional FP bearings have shown that the actual permanent displacement after earthquake excitation is approximately an order of magnitude less than the maximum possible permanent displacement [11]. Similar results were also observed by the authors in shaking table tests of a quarter-scale six-storey structure isolated with DCFP bearings. The isolation system in the study consisted of four equal radii equal friction DCFP bearings with $R_1 + R_2 - h_1 - h_2 = 3520$ mm and $\mu_{\min,1} \approx \mu_{\min,2} \approx 0.02$ in the prototype scale. Figure 13 shows the measured permanent displacements of the isolation system after unidirectional tests consisting of various historical earthquake records. The mean value of permanent displacement in the prototype scale for these 19 tests was 6 mm and the value predicted by Equation (24) is 70 mm, which is consistent with the results of previous studies.

5. CONCLUSIONS

To date, only DCFP bearings with equal radii and friction have been investigated [2–6]. In this case, the DCFP bearing behaves much like a traditional FP bearing with effective radius of curvature equal to the sum of the radii of curvature of the two concave surfaces (but modified for the height of the slider) and friction equal to the average of the coefficient of friction at each sliding interface. The displacements on each surface are equal in magnitude and equal to half of the total displacement. Accordingly, engineers have recognized that the primary advantage of employing DCFP bearings is the cost savings that can be achieved through their more compact size.

DOI: 10.1002/eqe

This paper has given a more general exposition of the behaviour of the DCFP bearing, especially in configurations where the radii of curvature and coefficients of friction of the two sliding surfaces are different. A generalized force–displacement relationship accounting for concave surfaces with different radii and friction as well as the effect of the articulated slider height has been presented. The fundamental principles and characteristics of the sliding motion have also been described. Data from characterization testing of bearings having configurations ranging from the typical case of equal radii and equal friction to the most general case of unequal radii and unequal friction have been shown to be in good agreement with the analytical predictions.

The presented analytical description of the behaviour of DCFP bearings revealed that, (a) the behaviour is in general, rigid-bilinear hysteretic and collapses to rigid-linear hysteretic for the case of equal coefficients of friction, (b) the height of the articulated slider affects the behaviour of the bearing in the sense that it reduces the effective radius of curvature to $R_1 + R_2 - h$, where h is the slider height, (c) the articulated slider undergoes relative rotation only in the case of different coefficients of friction at the two sliding interfaces and regardless of whether the two radii of curvature are equal or not, (d) friction tractions at the articulated slider can affect the behaviour of the bearing in the case of different coefficients of friction when motion on one surface ceases, and (e) the behaviour of DCFP bearings may be simulated by two single concave FP bearings models connected in series with a mass in-between representing the articulated slider.

Compared to a traditional FP bearing, the DCFP bearing offers a greater number of parameters affecting the force–displacement relationship that designers can vary. By employing concave surfaces with different coefficients of friction it was shown that a rigid-bilinear hysteretic relationship is achieved. Furthermore, even rigid-trilinear hysteretic behaviour is possible by using upper and lower concave plates with different displacement capacities. At large displacements, the slider would impact the retainer ring and stop sliding on one of the concave surfaces, but continue sliding on the other. This would cause an increase in the stiffness as the motion changes from sliding on both surfaces to only one. However, practical issues such as assessing and minimizing the effect of the impact on behaviour require further investigation.

Taking advantage of these extra design parameters, it may be possible to attain certain benefits in terms of performance that are not currently achievable. For example, a DCFP bearing with one surface having low friction and small radius paired with another surface of large radius and higher friction offers better re-centring capabilities for weak excitations but still has sufficient flexibility and energy dissipation capability for stronger excitations. In addition, configurations that minimize damage to secondary systems and non-structural components may also be possible. These possibilities warrant further research.

ACKNOWLEDGEMENTS

Financial support for this project was provided by the Multidisciplinary Center for Earthquake Engineering Research (Thrust Area 2, Task 8.2.1) and Earthquake Protection Systems, Inc., Vallejo, CA. This support is gratefully acknowledged.

REFERENCES

1. Touaillon J. *Improvement in Buildings*. United States Patent Office, Letters Patent No. 99,973, February 15, 1870.
2. Hyakuda T, Saito K, Matsushita T, Tanaka N, Yoneki S, Yasuda M, Miyazaki M, Suzuki A, Sawada T. The structural design and earthquake observation of a seismic isolation building using Friction Pendulum system.

DOI: 10.1002/eqe

Proceedings, *7th International Seminar on Seismic Isolation*, *Passive Energy Dissipation and Active Control of Vibrations of Structures*, Assisi, Italy, 2001.
3. Tsai CS, Chiang TC, Chen BJ. Experimental evaluation of piecewise exact solution for predicting seismic responses of spherical sliding type isolated structures. *Earthquake Engineering and Structural Dynamics* 2005; **34**(9):1027–1046. DOI: 10.1002/eqe.430.
4. Tsai CS, Chiang TC, Chen BJ. Experimental study for multiple Friction Pendulum system. *Proceedings*, *13th World Conference on Earthquake Engineering*, Vancouver, BC, Canada, 2004; Paper 669.
5. Tsai CS, Chiang TC, Chen BJ. Seismic behavior of MFPS isolated structure under near-fault earthquakes and strong ground motions with long predominant periods. *Proceedings*, *2003 ASME Pressure Vessels and Piping Conference*, vol. 1, Cleveland, Ohio, U.S.A., 2003; 73–79.
6. Tsai CS, Chiang TC, Chen BJ. Shaking table tests of a full scale steel structure isolated with MFPS. *Proceedings*, *2003 ASME Pressure Vessels and Piping Conference*, vol. 1, Cleveland, Ohio, U.S.A., 2003; 41–47.
7. Constantinou MC. Friction Pendulum double concave bearing. *NEES Report*, available at: http://nees.buffalo.edu/docs/dec304/FP-DC%20Report-DEMO.pdf, 2004.
8. Constantinou MC, Tsopelas P, Kasalanati A, Wolff ED. Property modification factors for seismic isolation bearings. *Technical Report MCEER-99-0012*, Multidisciplinary Center for Earthquake Engineering Research, State University of New York at Buffalo, Buffalo, NY, 1999.
9. Kasalanati A, Constantinou MC. Experimental study of bridge elastomeric and other isolation and energy dissipation systems with emphasis on uplift prevention and high velocity near source seismic excitation. *Technical Report MCEER-99-0004*, Multidisciplinary Center for Earthquake Engineering Research, State University of New York at Buffalo, Buffalo, NY, 1999.
10. American Association of State Highway and Transportation Officials. *Guide Specifications for Seismic Isolation Design*. AASHTO: Washington DC, 1999.
11. Tsopelas P, Constantinou MC, Kim YS, Okamoto S. Experimental study of FPS system in bridge seismic isolation. *Earthquake Engineering and Structural Dynamics* 1996; **25**(1):65–78. DOI: 10.1002/eqe.536.